Cell

Molecular Mechanism of Action of Plant DRM De Novo DNA Methyltransferases

Xuehua Zhong,[1,7,8] Jiamu Du,[2,8] Christopher J. Hale,[1] Javier Gallego-Bartolome,[1,3] Suhua Feng,[1,4] Ajay A. Vashisht,[5] Joanne Chory,[3,6] James A. Wohlschlegel,[5] Dinshaw J. Patel,[2,*] and Steven E. Jacobsen[1,4,*]

[1]Department of Molecular, Cell, and Developmental Biology, University of California, Los Angeles, Los Angeles, CA 90095, USA
[2]Structural Biology Program, Memorial Sloan-Kettering Cancer Center, New York, NY 10065, USA
[3]Plant Biology Laboratory, The Salk Institute for Biological Studies, La Jolla, CA 92037, USA
[4]Howard Hughes Medical Institute and Eli and Edythe Broad Center of Regenerative Medicine and Stem Cell Research, University of California, Los Angeles, Los Angeles, CA 90095, USA
[5]Department of Biological Chemistry, David Geffen School of Medicine, University of California, Los Angeles, Los Angeles, CA 90095, USA
[6]Howard Hughes Medical Institute, The Salk Institute for Biological Studies, La Jolla, CA 92037, USA
[7]Present address: Wisconsin Institute for Discovery, Laboratory of Genetics, University of Wisconsin, Madison, WI 53706, USA
[8]Co-first author
*Correspondence: pateld@mskcc.org (D.J.P.), jacobsen@ucla.edu (S.E.J.)
http://dx.doi.org/10.1016/j.cell.2014.03.056

SUMMARY

DNA methylation is a conserved epigenetic gene-regulation mechanism. DOMAINS REARRANGED METHYLTRANSFERASE (DRM) is a key de novo methyltransferase in plants, but how DRM acts mechanistically is poorly understood. Here, we report the crystal structure of the methyltransferase domain of tobacco DRM (NtDRM) and reveal a molecular basis for its rearranged structure. NtDRM forms a functional homodimer critical for catalytic activity. We also show that *Arabidopsis* DRM2 exists in complex with the small interfering RNA (siRNA) effector ARGONAUTE4 (AGO4) and preferentially methylates one DNA strand, likely the strand acting as the template for RNA polymerase V-mediated noncoding RNA transcripts. This strand-biased DNA methylation is also positively correlated with strand-biased siRNA accumulation. These data suggest a model in which DRM2 is guided to target loci by AGO4-siRNA and involves base-pairing of associated siRNAs with nascent RNA transcripts.

INTRODUCTION

DNA methylation is a conserved epigenetic gene regulation mechanism that is utilized by cells to regulate gene expression and suppress transposon activity. Unlike in mammals, where DNA methylation predominantly occurs in CG context (Lister et al., 2009), plant DNA is frequently methylated in three different sequence contexts: CG, CHG, and CHH (H = A, T, or C) (Law and Jacobsen, 2010). In *Arabidopsis thaliana*, while the maintenance of CG and CHG methylation is primarily controlled by METHYLTRANSFERASE1 (MET1, an ortholog of mammalian Dnmt1) and CHROMOMETHYLASE3 (CMT3, a plant-specific methyltransferase), respectively (Du et al., 2012; Finnegan and

Dennis, 1993; Finnegan and Kovac, 2000; Lindroth et al., 2001; Stroud et al., 2013), the maintenance of CHH methylation is controlled by DOMAINS REARRANGED METHYLTRANSFERASE2 (DRM2, an ortholog of mammalian Dnmt3) (Law and Jacobsen, 2010) and CMT2 (Stroud et al., 2014; Zemach et al., 2013).

De novo DNA methylation in all sequence contexts is mediated by DRM2 and is dependent on RNAi-like machinery via a process termed RNA-directed DNA methylation (RdDM) (Law and Jacobsen, 2010). This pathway involves two main phases: an upstream small interfering RNA (siRNA) biogenesis phase and a downstream methylation targeting phase. Biogenesis of siRNAs is initiated by a plant-specific RNA polymerase IV (Pol IV), which generates single-stranded RNA transcripts that are copied into double-stranded RNA by an RNA-dependent RNA polymerase 2 (RDR2). The resulting transcripts are cleaved into 24 nt siRNAs by a Dicer-like endonuclease 3 (DCL3) and further loaded into ARGONAUTE 4 (AGO4) forming AGO4-siRNA complexes. The targeting phase involves another plant-specific RNA polymerase, polymerase V (Pol V), which produces noncoding RNA transcripts that are proposed to act as a scaffold to recruit AGO4 through base-pairing of associated siRNAs (Law and Jacobsen, 2010; Wierzbicki et al., 2009). While genome-wide occupancy of Pol V is dependent on the DDR complex consisting of DEFECTIVE IN MERISTEM SILENCING 3 (DMS3), DEFECTIVE IN RNA-DIRECTED DNA METHYLATION 1 (DRD1), and RNA-DIRECTED DNA METHYLATION 1 (RDM1) (Zhong et al., 2012), chromatin association of Pol IV is partially dependent on an H3K9 methyl binding domain protein, SHH1/DTF1 (Law et al., 2013; Zhang et al., 2013). A recent study suggests that DNA methylation is also required for Pol V association to chromatin, demonstrating the nature of the RdDM pathway as a self-reinforcing loop mechanism (Johnson et al., 2014). The co-occurrence of Pol IV-dependent siRNAs and Pol V-dependent noncoding RNA transcripts is thought to determine the sites of DRM2 action. However, despite the identification of a large number of proteins required for the RdDM pathway, the specific mechanism of DRM2 action, including its biochemical activities, interacting

CrossMark

A

B
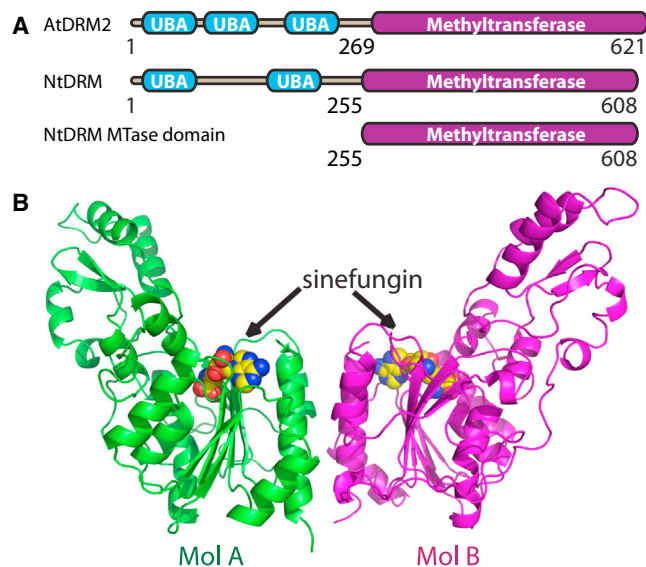
Figure 1. Overall Structure of NtDRM

(A) Color-coded domain architecture of AtDRM2, NtDRM, and NtDRM MTase domain used to grow crystal. UBA stands for ubiquitin-associated domain.

(B) Ribbon representation of the overall structure of NtDRM MTase domain dimer with bound sinefungin. One monomer (Mol A) is colored in green and the other one (Mol B) in magenta. The sinefungin cofactors bound to each monomer are shown in space-filling model.

See also Figure S1 and Table S1.

partners, and how DRM2 is recruited to specific loci, remains largely unknown.

To further understand the molecular mechanism of DRM2 action, we carried out structural and functional studies. We solved the crystal structure of the methyltransferase domain of a DRM2 homolog from tobacco, NtDRM. The structure reveals that although DRM proteins have a rearrangement of their methyltransferase sequence motifs, the overall structure retains a classic class I methyltransferase fold (Schubert et al., 2003). In the crystal, NtDRM forms a homodimer with the dimer interface mimicking the mammalian Dnmt3a-Dnmt3L heterodimer interface. Mutations disrupting this dimerization significantly reduce its in vitro methyltransferase activity, which is similar to the behavior of Dnmt3a-Dnmt3L. These results suggest that dimerization may be a commonly used mechanism to initiate DNA methylation. To further understand the mechanism of DRM2 action, we performed affinity purification followed by mass spectrometry and found that *Arabidopsis* AGO4 copurified with DRM2. Given that AGO4 binds siRNAs, and that siRNAs have the potential to base pair with either the complementary DNA strand or nascent RNA transcripts, we examined the relationship between the strandedness of DNA methylation and siRNAs. We found that strand-biased DNA methylation is positively correlated with strand-biased siRNAs, suggesting that DRM2 preferentially methylates the template DNA strand for Pol V transcription. Collectively, our data suggest a model wherein AGO4-siRNAs guide a DRM2 dimer to methylate a template DNA strand for Pol V transcription and this process is mediated by base-pairing of associated siRNAs with Pol V transcripts.

RESULTS AND DISCUSSION

Overall Structure of the NtDRM Catalytic Domain

To begin to reveal the mechanism of DRM action, we sought to determine the crystal structure of DRM2. Despite extensive efforts to crystallize *Arabidopsis* DRM2, we failed to obtain diffraction quality crystals. Instead, we successfully crystallized the DRM methyltransferase domain from a related plant, *Nicotiana tabacum* (NtDRM MTase, residues 255–608). NtDRM shares a similar domain architecture and function with DRM2 (Figure 1A) (Wada et al., 2003). The structure of NtDRM MTase in complex with sinefungin, an analog of the cofactor substrate S-adenosyl-L-methionine (SAM), was solved by the SAD method and refined to 2.8 Å resolution yielding an *R* factor of 20.1% and a free *R* factor of 22.1%. In the asymmetric unit, there is an NtDRM MTase dimer with each molecule bound to a cofactor analog sinefungin in the active site (Figure 1B; Table S1 available online). Overall, the protein exhibits well-defined electron density, except that the catalytic loop regions (residues 567–584 in monomer A and residues 569–584 in monomer B) were not well defined and we were unable to build these segments into the final model. The NtDRM MTase dimer exhibits a butterfly-like arrangement with the two monomers related by a 2-fold noncrystallographic symmetry axis. The two catalytic domains dimerize in the middle, and the two target recognition domains (TRDs) extend on two sides as the wings (Figure 1B).

The extreme N-terminal 30 residues of NtDRM MTase (residues 259–288) form a long loop wrapped on the surface of the core methyltransferase domain, which is composed of the remaining residues (residues 289–608). Although the primary sequence of NtDRM MTase (and all other DRM2 proteins) is rearranged as compared to that of class I methyltransferases, its overall structure adopts a typical class I methyltransferase fold with a catalytic domain and a TRD domain (Figures 2A and 2B). The catalytic domain features a central seven-stranded β sheet flanked by one layer of three α helices on one side and another layer of four α helices on the other side (Figures 2A and 2B) resembling other class I DNA methyltransferases including M.HhaI, Dnmt3a, Dnmt1, and ZMET2 (Cheng et al., 1993; Du et al., 2012; Jia et al., 2007; Song et al., 2011) (Figure 2C). The catalytic loop of NtDRM is disordered, probably due to the absence of the substrate DNA. In the region near the catalytic domain, the TRD domain of NtDRM is composed of a two-stranded antiparallel β sheet similar to that of Dnmt3a. In the region away from the catalytic domain, the TRD domain has two antiparallel α helices connected by a loop, which defines an arrangement of the TRD domain (Figures 2A and 2C), indicating a DNA substrate binding mode different from other known DNA methyltransferases.

The Rearranged Domain Structure of DRM

The first residue of the core methyltransferase domain, Pro288, is adjacent to the C-terminal end of the protein in three-dimensional space (Figures 2A and 2C). Similarly, the N and C termini of Dnmt3a are also adjacent to each other (Figure 2C). If the N and C termini of NtDRM MTase were fused together as a closed loop and then broken around Gly480 (black arrow in Figure 2B), then its sequence folding topology would be identical to Dnmt3a.
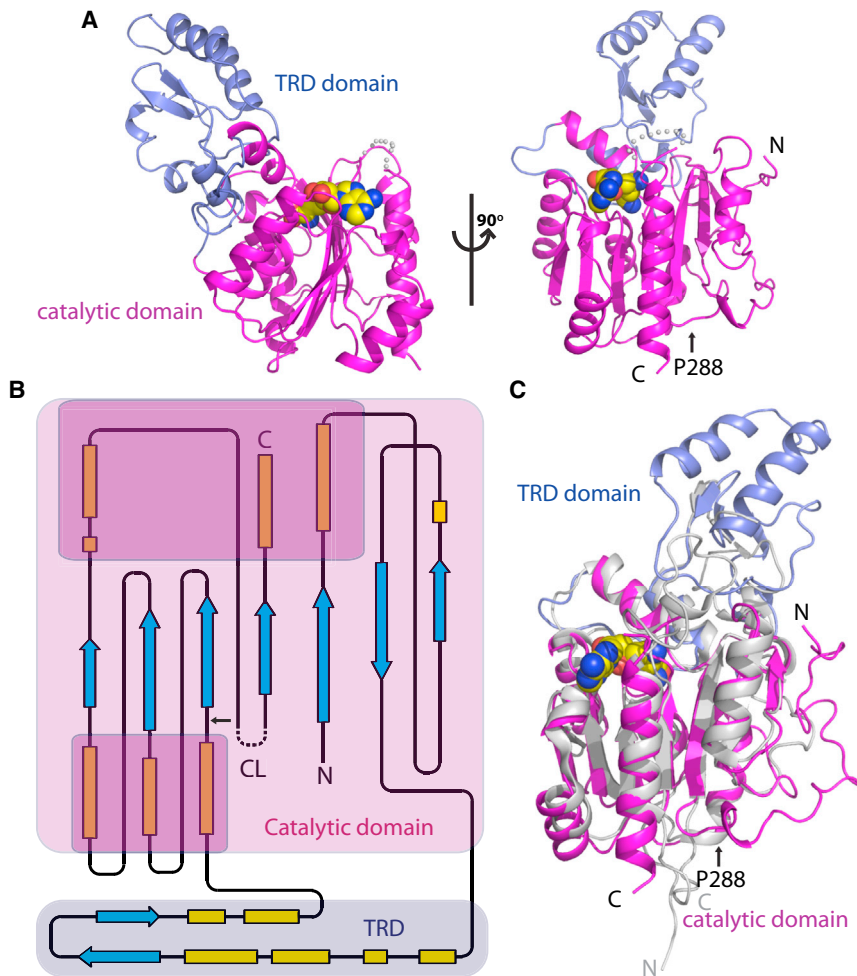
Figure 2. Structural Basis of the Domain Rearrangement Mechanism

(A) The structure of NtDRM MTase in two orientations rotated by 90°. The catalytic domain is colored in magenta and the TRD in blue.

(B) The schematic representation of the secondary structural assembly of NtDRM. The catalytic domain and TRD are as indicated, respectively. The disordered catalytic loop (CL) is shown by a dashed line. The break point corresponding to the N and C termini of Dnmt3a is indicated by an arrow.

(C) Superposition of NtDRM monomer with Dnmt3a. NtDRM is colored the same as in Figure 2A, and Dnmt3a is in silver. The N and C termini of the two proteins are indicated, respectively. The initiation site of NtDRM MTase domain, Pro288, is highlighted to be near the C terminus of the protein.

Thus, while the DRM MTase domains are rearranged in the linear sequence, it retains the overall fold of a classic class I methyltransferase. The domain rearrangement mechanism confirms previous speculation that DRM folds similarly to other typical class I methyltransferases despite the motif rearrangement (Cao et al., 2000). The point of rearrangement is identical in many plant species, at the bottom side of the catalytic domain opposite against and far away from the catalytic center or the cofactor binding site of the catalytic and TRD domains (Figure 2; Figure S1), suggesting that the rearrangement occurred during an early stage of plant evolution. Based on structures, it seems likely that DRM proteins have a catalytic mechanism similar to other class I methyltransferases.

NtDRM MTase Forms a Functional Homodimer Critical for Catalytic Activity

It was reported that mammalian Dnmt3a and Dnmt3L form a Dnmt3L-Dnmt3a-Dnmt3a-Dnmt3L tetramer and that this oligomeric status is essential for its DNA methylation activity (Jia et al., 2007). A Dnmt3a F728A mutant, disrupting the Dnmt3a-Dnmt3L heterodimer interface, abolishes the methyltransferase activity (Jia et al., 2007). Interestingly, when we superpose

Dnmt3a onto one monomer of the NtDRM MTase dimer, we found that the other monomer of the NtDRM MTase dimer can be well superposed with the Dnmt3a-dimerized Dnmt3L molecule (Jia et al., 2007) (Figure 3A). The NtDRM MTase homodimer interface mimics the Dnmt3a-Dnmt3L heterodimer interface, with the former stabilized by a hydrophobic core composed of aromatic amino acids Phe310 and Tyr590 from each monomer and a hydrophilic periphery involved in salt bridges and hydrogen bond interactions between positively charged Arg309 and Arg605 and negatively charged Asp591 and Glu283 (Figure 3B). However, no interface of NtDRM MTase mimics the Dnmt3a-Dnmt3a interface in the crystal, indicating that, unlike the Dnmt3a-Dnmt3L that forms a heterotetramer, DRM likely utilizes a homodimer as a functional unit. By analyzing plants containing two different DRM2 constructs with different epitope tags, we also confirmed that DRM forms multimers in vivo (Figure 3C), consistent with the structural data.

To determine the importance of NtDRM dimerization, we mutated all the residues involved in the dimerization to serine (E283S/R309S/F310S/Y590S/D591S, designated as NtDRM-M5) and solved the crystal structure of the mutant protein (Table S1). The overall structure of NtDRM-M5 monomer is almost identical to the wild-type NtDRM MTase with a root-mean-square deviation of only 0.77 Å for 326 aligned Cα atoms by aligning their monomer structures (Figure S2A); however, the dimer interface of NtDRM MTase is completely disrupted. In addition, enzymatic activity assays show that NtDRM-M5 has lost virtually all DNA methyltransferase activity compared with the wild-type protein (Figure 3D). This result indicates that, like the Dnmt3a-Dnmt3L interface, the DRM dimer interface is essential for catalysis. One plausible explanation is that dimerization might help stabilize the conformation of the catalytic loop because the C-terminal portion of the active site loop is involved in dimer interface
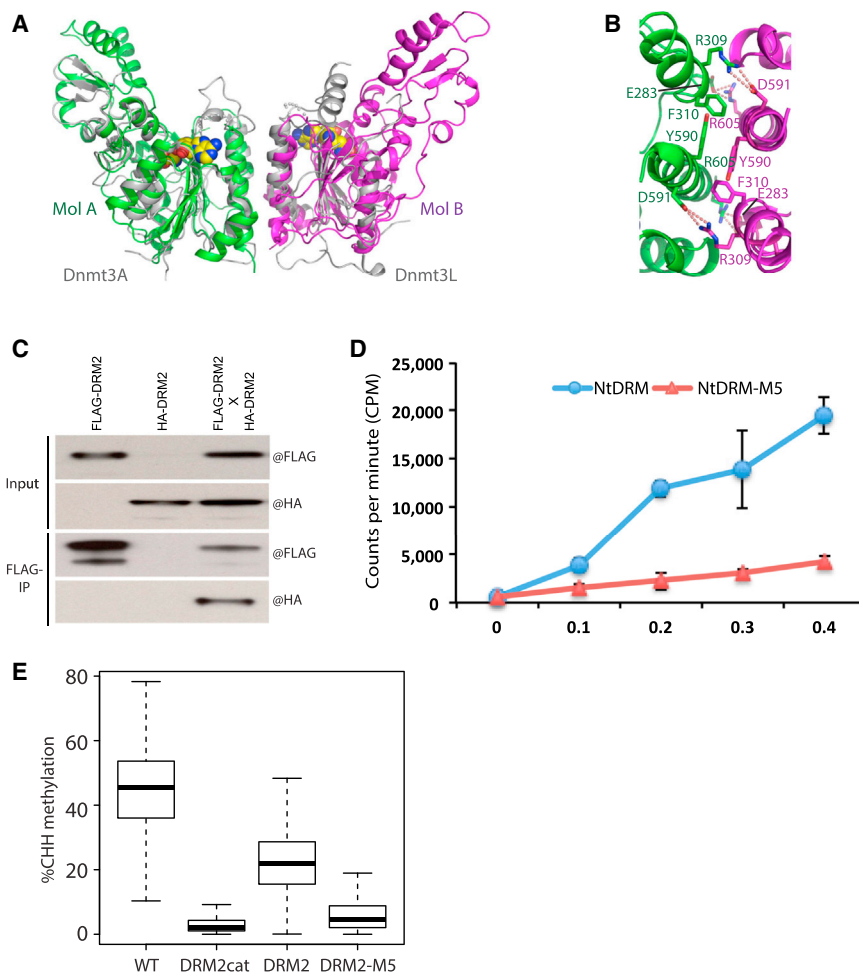
Figure 3. NtDRM MTase Forms a Homodimer, and Dimerization Is Required for Catalytic Activity

(A) Upon superposition of Dnmt3a with one monomer of NtDRM MTase, the other NtDRM MTase monomer can be well superposed with the Dnmt3a dimerized Dnmt3L. NtDRM MTase is colored as in Figure 1B, and Dnmt3a-Dnmt3L dimer is in silver.

(B) Detailed interaction of the NtDRM MTase homodimer interface. The interacting residues are shown in stick representation, and hydrogen bonds are shown by dashed red lines.

(C) Coimmunoprecipitation assays confirming that DRM2 forms multimers in *Nicotiana benthamiana*.

(D) In vitro methyltransferase activity assays on NtDRM MTase and dimerization-disrupting mutant NtDRM-M5. Error bars represent SD for three replicates.

(E) Boxplot of CHH methylation at *drm2* CHH hypomethylated DMRs in wild-type (WT), a *drm2* mutant transformed with a catalytic mutant *DRM2* transgene (*DRM2cat*), a wild-type transgene (*DRM2*), and a dimerization disruptive mutant (*DRM2-M5*).

See also Figures S2 and S3 and Table S2.

domain and the catalytic site of NtDRM MTase form a large continuous positively charged surface suitable for DNA substrate binding (Figure S3A). Despite extensive efforts, we were not able to crystallize NtDRM with DNA oligomer duplexes of varying length and overhangs. We instead modeled the NtDRM MTase with a DNA substrate based on the structure of the productive covalently linked Dnmt1-DNA complex (Song et al., 2012). The model reveals that the substrate DNA duplex can be positioned within the substrate cleft between the catalytic domain and TRD, with the looped out to-be-methylated cytosine base positioned within the active site near the cofactor analog sinefungin (Figure S3B). The two α helices of the TRD approach the major groove of the putative substrate DNA duplex, most likely participating in binding and sequence-specific DNA recognition (Figure S3B). Given that this model predicts that NtDRM is most likely sufficient to capture the substrate DNA duplex, it appears unnecessary to form a Dnmt3a-Dnmt3a like dimer to enlarge the DNA binding surface. This may explain why only the Dnmt3a-Dnmt3L surface is conserved in NtDRM, while the Dnmt3a-Dnmt3a surface is not present in NtDRM.

Collectively, our results reveal a possible conserved dimerization mechanism for plant and animal de novo DNA methyltransferases, suggesting that dimerization may be a commonly used mechanism to initiate DNA methylation.

UBA Domains Are Important for DRM Function In Vivo

Besides the methyltransferase domain, DRM proteins also contain ubiquitin-associated (UBA) domains (Figure 1A) of unknown function (Cao et al., 2000). Previously, DRM2 UBA domains were

formation (Jia et al., 2007). To further examine the functional significance of DRM2 dimerization in vivo, we generated a transgenic version of DRM2 in which the five key residues involved in dimerization were mutated to serine (E301S, R327S, H328S, F610S, and E611S), designated as DRM2-M5. The wild-type *DRM2* (*DRM2*) and mutant *DRM2* (*DRM2-M5*) transgenes were transformed into *drm1 drm2*, and the effects of loss of DRM2 dimerization on DNA methylation were assessed by a whole-genome bisulfite sequencing approach. As shown in Figure 3E, DNA methylation was significantly reduced in a *DRM2-M5* mutant line compared to that of wild-type *DRM2* lines even though they show similar expression levels of the DRM2 transgene (Figure S2B). This result suggests that dimerization is also critical for in vivo DRM2 activity.
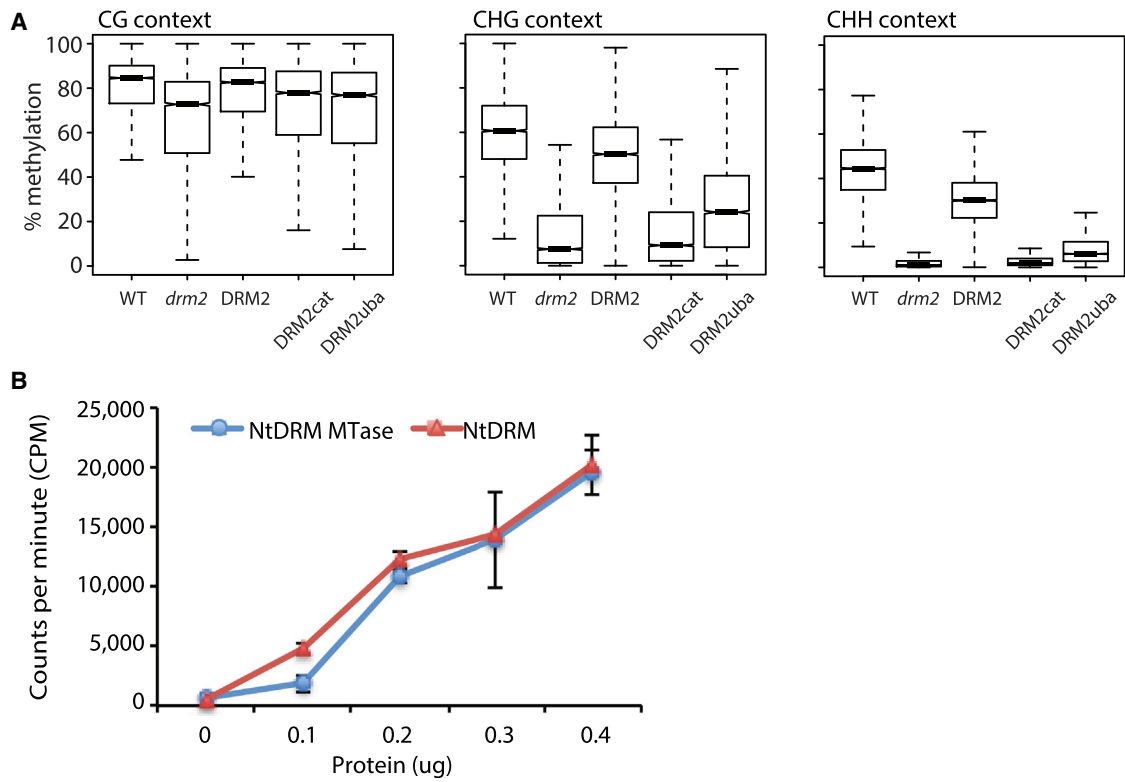
Besides the Dnmt3a-Dnmt3L heterodimer interface, the Dnmt3a-Dnmt3a homodimer interface was also reported to be essential for the catalytic activity of Dnmt3a (Jia et al., 2007). Dnmt3a has one of the smallest TRD domains in comparison to other DNA methyltransferases. However, the dimerization of two Dnmt3a molecules doubles the DNA binding surface and enables the DNA substrate to be more accessible to the enzyme (Jia et al., 2007). In our NtDRM MTase structure, the TRD domain is larger than that of Dnmt3a (Figure 2C). In addition, the TRD

Figure 4. UBA Domains Are Required for Global DNA Methylation
(A) Boxplots showing the DNA methylation at CG, CHG, and CHH contexts for wild-type (WT), *drm2* mutant, or wild-type *DRM2*, catalytic mutant (*DRM2cat*), or UBA mutant (*DRM2uba*) transformed back into *drm2*, respectively.
(B) In vitro methyltransferase activity assays on full-length NtDRM and truncated NtDRM with catalytic domain (NtDRM MTase). Error bars represent SD for three replicates.
See also Figure S4.

shown to be required for the maintenance of DNA methylation at the *MEA-ISR* locus (Henderson et al., 2010). However, it remains unclear to what extent UBA domains are required for DNA methylation in the genome. To address these questions, we first examined whether the UBA domains are required for global DNA methylation in vivo. We performed whole-genome bisulfite sequencing on previously published *DRM2uba* mutant lines where conserved residues within UBA domains were mutated and the *DRM2uba* mutant transgene was transformed into a *drm2* null mutant (Henderson et al., 2010). As shown in Figure 4A, DRM2uba showed a strong global loss of DNA methylation that was only slightly weaker than a catalytically inactive DRM2cat mutant (negative control), indicating that the UBA domains are required for genome-wide DRM2 activity in vivo. We further showed that loss of DNA methylation in DRM2uba is unlikely due to reduced expression of DRM2, since DRM2uba has a similar protein level as that of wild-type DRM2 (Figure S4D).

It is possible that the failure in DNA methylation restoration by DRM2uba is due to the loss of DRM2 catalytic activity. Despite extensive testing, we have been unable to find in vitro conditions that allow for robust *Arabidopsis* DRM2 activity. Thus, we compared the activity of the full-length NtDRM with the truncated NtDRM containing only the catalytic domain used for crystallization. As shown in Figure 4B, the NtDRM MTase domain
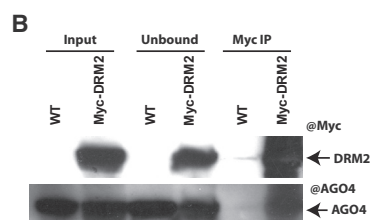
alone exhibited activity very similar to that of the full-length NtDRM, suggesting that UBA domains are not necessary for DRM catalytic activity. It is therefore possible that the UBA domains are involved in other aspects of DRM function, such as targeting DRM to specific loci. Consistent with this possibility, we noted a bimodal distribution of methylation change in the DRM2uba line as compared to that of DRM2cat (Figure S4A), suggesting that some DRM2 target sites are more sensitive to the loss of the UBA domains than others. Furthermore, we note that the sites most strongly hypomethylated in the DRM2uba line tend to have less broadly distributed heterochromatic marks than those sites weakly affected in a DRM2uba mutant (Figures S4B and S4C), suggesting that the UBA domains may help reinforce DRM2 activity at euchromatic regions of the genome that contain smaller patches of heterochromatin.

AGO4 Copurifies with DRM2 In Vivo

To further explore the biochemical activity of DRM2, we performed immunoprecipitation and mass spectrometry (MS) to identify DRM2-interacting proteins. We generated an epitope-tagged *9xMYC-biotin ligase recognition peptide* (*BLRP*)-*DRM2* transgenic line where the expression of DRM2 is under the control of its own promoter. After affinity purification, copurifying proteins were identified through MS analysis. Peptides

A

	Experiment I				Experiment II			
	Spectra	Unique Peptides	% Coverage	NSAF	Spectra	Unique Peptides	% Coverage	NSAF
DRM2	310	37	43.3	1025	331	32	45.8	2500
At2g27040 (AGO4)	35	20	22.1	78	15	8	10.4	77
At5g03740 (HD2C)	11	6	25.8	79	5	3	11.8	82
At5g21150 (AGO9)	11	10	12.9	25	4	2	2.5	21
At3g16830	11	7	5.4	20	5	5	4.6	21
At2g19520 (MSI4)	25	8	21.3	75	3	2	5.9	28
At3g45980 (HTB9)	10	5	35.3	138	12	5	35.3	379
At1g75950	4	2	17.5	51	2	2	13.8	59

MS analyses of DRM2 purifications (Only proteins present in both experiments are shown)

B

Figure 5. DRM2 Is Associated with AGO4 In Vivo

(A) Summary of proteins associated with DRM2 identified by MS. Only proteins represented in both replicas are shown. NSAF, normalized spectral abundance factor.

(B) Affinity purification confirming DRM2-AGO4 interaction.

corresponding to AGO4 (At2g27040) were the most abundant in two independent purifications (Figure 5A). Less abundant peptides from a few other proteins were also found in both replicas (Figure 5A), although the biological significance of these interactions has not been tested. We validated the interaction between DRM2 and AGO4 by performing MYC pull-down assays in which tagged DRM2 was isolated using immobilized MYC beads and the presence of AGO4 in the purified DRM2 fraction was examined with an AGO4 endogenous antibody (Figure 5B). Taken together, the MS analyses, together with affinity purification data, indicate that DRM2 is associated with AGO4 in vivo.

DRM2 Mediates Strand-Biased DNA Methylation that Is Positively Correlated with Strand-Biased siRNAs

Given that AGO4 binds siRNAs (Qi et al., 2006) and interacts with DRM2 (Figure 5), we sought to examine the relationship between DRM2-dependent methylation and siRNA populations. Genomic studies have established a strong correlation between endogenous siRNAs and DRM2-mediated DNA methylation throughout the genome (Cokus et al., 2008; Law et al., 2013; Lee et al., 2012; Lister et al., 2008). However, the mechanism by which siRNAs guide DRM2 methylation is poorly understood. Previous observations of strand-biased DNA methylation that tended to associate with siRNAs in *Arabidopsis* (Lister et al., 2008; Luo and Preuss, 2003) prompted us to investigate DRM2 sites and to specifically test whether there is a relationship between siRNA strandedness and the respective strand of targeted cytosines. To this end, we used a set of previously identified DRM2-dependent total siRNA clusters (Law et al., 2013) and defined a subset of these clusters that showed a strand-biased distribution of siRNAs as well as clusters that showed little to no strand bias. Strand-biased clusters were defined as having a significant

excess of siRNA reads mapping to either the positive or negative strand relative to the complementary strand (see Experimental Procedures). We then used previously published whole-genome bisulfite sequencing data sets (Law et al., 2013) to calculate strand bias of both the methylcytosine and cytosine content at these clusters. As shown in Figure 6A, the strand-biased siRNA clusters were correlated with a strand bias for both cytosine content and methylcytosine content. Moreover, the direction of the bias was the same between siRNAs and cytosines or methylcytosines (Figure 6B; Figure S5A), consistent with the general trend previously noted in the whole-genome bisulfite sequencing data (Lister et al., 2008). Thus, positive-strand siRNA clusters correlated with regions with a positive strand bias for methylcytosine and total cytosine content and vice versa. These results suggest that DRM2 preferentially methylates the same DNA strand as the siRNA, rather than the complementary strand to which the siRNA could base pair.

As a confirmation of these results, we used whole-genome bisulfite sequencing data from a *drm2* mutant line to define individual cytosines whose methylation was most strongly lost upon loss of DRM2 (Figure 6C). We then plotted 24 nt siRNA abundance around these cytosines. Similar to what we observed at strand-biased siRNA clusters, we noted that siRNA abundance at these differentially methylated cytosines strongly correlated with the strandedness of the methylcytosine assayed; differentially methylated cytosines on a given strand are more likely to be covered by siRNAs of the same strand as opposed to siRNAs of the complement strand (Figure 6D). We also noticed a pattern in the abundance of siRNA 5′ ends distributed around differentially methylated cytosines, with the highest abundance of 5′ ends 23 nt upstream of the cytosine in question (Figure 6D). In other words, the strongest 24 nt siRNA signal at differentially methylated cytosines correlates to a strand-matched siRNA positioned such that the 3′ nt of the siRNA corresponds to the cytosine methylated by DRM2. One possible trivial explanation for this result is that, because 24 nt siRNAs have an overrepresentation of cytosines at their 3′ end (Figure S5B), by centering our analysis on a cytosine, we may be identifying patterns that are simply a consequence of the underlying sequence composition of the Arabidopsis 24 nt siRNA population. Alternatively, it is possible that AGO4 and the associated 24 nt siRNAs are physically positioning the DRM2 active site to the targeted cytosine,
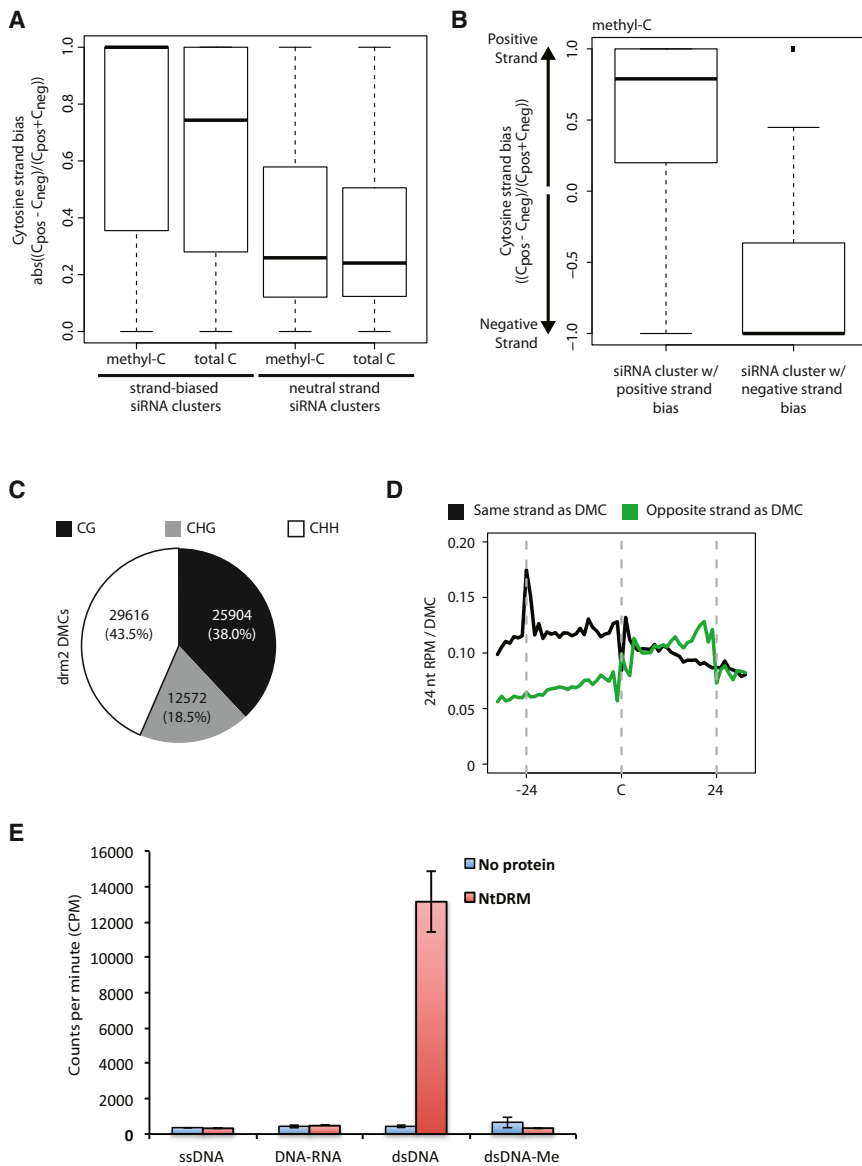
Figure 6. siRNA Strand Biases Are Correlated with DNA Methylation Strand Biases

(A) Separation of DRM2-dependent siRNA clusters into strand-biased siRNA clusters and clusters with no strand bias, and assessment of methylcytosine and cytosine strand bias over these clusters.

(B) The direction of methylcytosine strand bias correlates with the direction of siRNA strand bias at strand-biased siRNA clusters.

(C) Number and context of identified hypomethylated differentially methylated cytosines (DMCs) in a *drm2* mutant.

(D) Plot of the relative number of 24 nt siRNA 5′ ends around *drm2* DMCs for siRNAs homologous to the same strand as the DMCs or the opposite strand.

(E) NtDRM exhibits robust methyltransferase activity on duplex DNA templates, but not on single-stranded DNA or RNA-DNA hybrids. ssDNA, single-stranded DNA; DNA-RNA, DNA and RNA hybrid; dsDNA, double-stranded DNA; dsDNA-Me, double-stranded control premethylated DNA. Error bars represent SD for three replicates.

See also Figure S5.

et al., 2009). These observations suggest models in which DRM2 might directly methylate single-stranded DNA or perhaps DNA-RNA hybrids produced by annealing of the Pol V RNA transcript with the complementary DNA strand (Figures 7A and 7B). To shed additional light on these potential models, we performed in vitro methylation reactions with NtDRM MTase using a variety of templates. We observed robust methylation on a dsDNA template, but not on single-stranded DNA or DNA-RNA hybrids (Figure 6E). Therefore, it seems likely that despite being targeted by siRNAs and nascent noncoding Pol V RNAs, DRM2 is likely methylating duplex DNA. In order to reconcile this

which could also explain the overrepresentation of cytosine at 24 nt 3′ ends. In support of this latter hypothesis, we observed that the pattern of siRNA strandedness is much greater for *drm2* DMCs as compared to DMCs defined in other methyltransferase mutants that are presumed to operate largely independent from siRNA pathways (Figures S5C–S5E).

DRM2 Preferentially Methylates Double-Stranded DNA Templates

The observation that preferentially DRM2-targeted cytosines correlate with the same strand as RdDM-associated siRNAs suggests that the targeting of DRM2 enzymatic activity by these RNAs is likely through a mechanism other than direct base-pairing between the siRNA and its complementary DNA sequence. Furthermore, previous work suggests that AGO4 and its associated siRNAs interact with nascent Pol V transcripts (Wierzbicki

observation with the strand-biased nature of siRNA-guided DNA methylation, we hypothesize that the tethering of the AGO4-siRNA complex to a Pol V transcript positions DRM2 to methylate the Pol V template strand of DNA near the Pol V exit channel, where perhaps the structure of the Pol V complex or associated proteins allows for the transfer of strand information for DRM2 target selection (Figure 7C). This hypothesis is consistent with previous observations that AGO4 is physically associated with the CTD of Pol V (El-Shami et al., 2007; Li et al., 2006). In this model, AGO4 would acts as a bridge between the siRNA-Pol V transcript and DRM2.

Conclusions

The results reported here provide molecular details on the functioning of plant de novo DNA methyltransferases. Our structural data reveal that despite its rearranged structure, DRM shares a

A

B

C
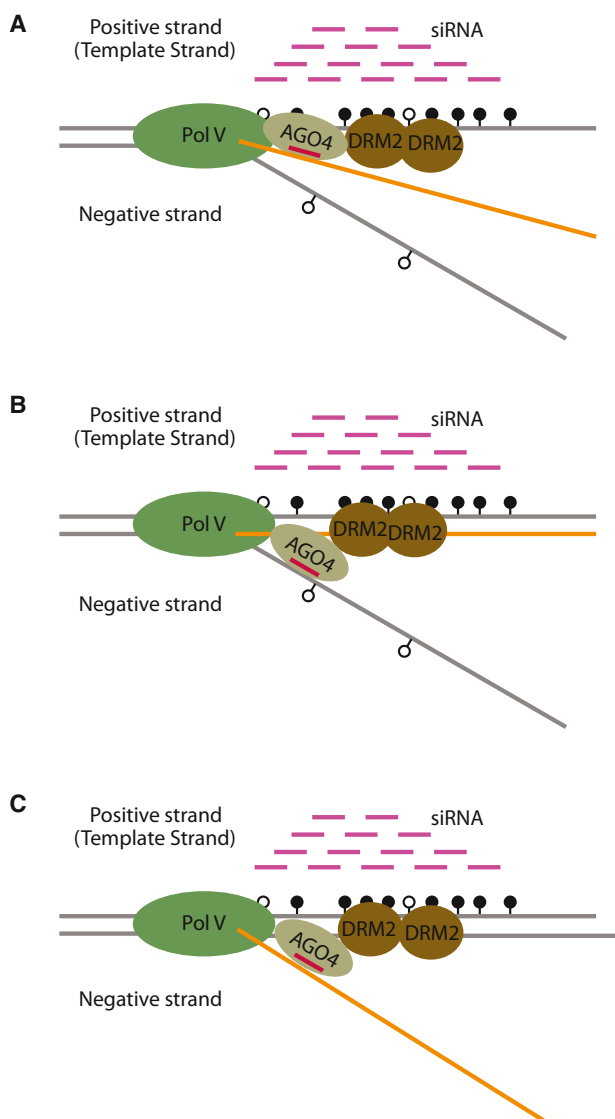
Figure 7. Models for the Strand-Specific Nature of DRM2 Methylation

(A) DRM2 activity on single-stranded DNA exposed by Pol V transcription. The activity would be positioned by DRM2's interaction with AGO4, as well as the AGO4-siRNA interaction with Pol V and base-pairing to the nascent Pol V transcript (orange).

(B) DRM2 activity on a RNA-DNA hybrid formed by interaction between the Pol V transcript and template DNA strand. DRM2 activity is positioned by the interaction with AGO4 and the AGO4-siRNA interaction with Pol V and base-pairing to the coding DNA strand displaced by Pol V transcription.

(C) DRM2 activity on a double-stranded DNA template formed immediately after passage of the transcription bubble wherein DRM2 activity and strand selection is mediated by an interaction with AGO4. The AGO4-siRNA complex would be mediated by an interaction with Pol V and base-pairing with the nascent Pol V transcript.

The solid and open lollipops in (A)–(C) represent methylated and unmethylated cytosines, respectively.

classic class I methyltransferase fold with other known class I methyltransferases. We also uncovered that DRM forms a homodimer and that dimerization is essential for catalytic activity

and in vivo function. These results suggest a conserved mechanism for eukaryotic de novo DNA methyltransferases, in which dimerization is commonly used to initiate DNA methylation. A key finding from our in vivo analysis is that DRM2 interacts with AGO4 and that DRM2-mediated strand-biased DNA methylation is correlated with strand-biased siRNAs. These results are consistent with a model in which DRM2 is acting on DNA immediately after Pol V transcription such that one of the two DNA strands is a preferential target.

EXPERIMENTAL PROCEDURES

Plant Materials

The *drm1/2* mutant plants were previously described (Cao and Jacobsen, 2002). Myc-DRM2, Myc-DRM2cat, and Myc-DRM2uba transgenic lines were previously described (Henderson et al., 2010).

Construction of Vectors and Generation of Transgenic Plants

DNA fragments containing *NtDRM MTase* and *NtDRM MTase-M5* were amplified by PCR and were cloned into pENTRD_TOPO vector (Invitrogen) to create pENTRD_*NtDRM* and pENTRD_*NtDRM-M5*. These constructs were recombined into the binary vectors pEarleyGate202 and pEarleyGate201 (Earley et al., 2006) to create FLAG and hemagglutinin (HA) fusions, respectively. Each construct was then introduced into *Agrobacterium* AGL1 cells, which were used subsequently to infiltrate leaves of *Nicotiana benthamiana*. A pENTRD vector containing a genomic fragment of *DRM2* with N-terminal fusion of 3xFLAG-9xMYC was mutated to generate *DRM2-M5* mutant lines using the multiquick change kit (Stratagene). These constructs were recombined into a modified pEarlyGate302 binary vector as previously described (Du et al., 2012). These constructs were transformed into *drm1 drm2* mutant. Detailed information for oligos can be found in Table S2.

Protein Preparation

A construct encoding the *Nicotiana tabacum* DRM MTase domain (255–608) was inserted into a self-modified vector, which fuses an N-terminal hexahistidine plus a yeast sumo tag to the target gene. The plasmid was transformed into *E. coli* strain BL21 (DE3) RIL (Stratagene). The cells were cultured at 37°C until optical density 600 reached 1.0, and then the media was cooled to 17°C and 0.2 mM isopropyl β-D-1-thiogalactopyranoside was added to induce protein expression overnight. The hexahistidine-sumo-tagged protein was initially purified using a HisTrap FF column (GE Healthcare). Then, the tag was cleaved by Ulp1 protease, which was subsequently removed by a second step HisTrap FF column purification. The pooled target protein was further purified by a Heparin FF column (GE Healthcare) and a Hiload Superdex G200 16/60 column (GE Healthcare) with buffer 300 mM NaCl, 20 mM Tris (pH 8.0), and 5 mM DTT. The Se-methionine substituted protein was expressed in Se-methionine (Sigma) containing M9 medium and purified using the same protocol as the wild-type protein. The *NtDRM-M5* (*E283S/R309S/F310S/Y590S/D591S*) mutant was generated using a Phusion Site-Directed Mutagenesis Kit (New England Biolabs) and was expressed and purified with the same protocol as the wild-type protein. For enzymatic assays, full-length *NtDRM* (1–608) was cloned into the same vector and expressed and purified with the same protocol as the MTase domain.

Crystallization

Before crystallization, the purified proteins were concentrated to 8 mg/ml and mixed with sinefungin at a molar ratio of 1:3 at 4°C for 30 min. Crystallization was conducted at 20°C using the hanging drop vapor diffusion method. The wild-type NtDRM MTase was crystallized under 0.19 M CaCl$_2$, 5% glycerol, 26.6% PEG400, and 0.095 M HEPES (pH 7.5) conditions. The Se-methionine-substituted NtDRM MTase was crystallized under 4.5 M NaCl, and 0.1 M HEPES (pH 7.5) conditions. The NtDRM^{M5} was crystallized under 0.2 M sodium nitrate, 20% PEG3350, and 0.1 M BisTris propane (pH 7.5) conditions. All the crystals were soaked into the reservoir solution supplement with 15% glycerol for 1 min. Then, the crystals were mounted on a nylon loop and

flash-cooled into liquid nitrogen. The diffraction data for the Se-methionine-substituted NtDRM MTase were collected at beamline BL17U (Shanghai Synchrotron Radiation Facility in Shanghai, China). The diffraction data for the wild-type and mutant NtDRM MTase were collected at beamline 24IDE (Advanced Photon Source at the Argonne National Laboratory in Chicago, IL). All the data were processed with the program HKL2000 (Otwinowski and Minor, 1997). The statistics of the diffraction data are summarized in Table S1.

Structure Determination and Refinement

The structure of NtDRM MTase in the presence of sinefungin was solved using single-wavelength anomalous dispersion method as implemented in the program Phenix (Adams et al., 2010). The model building was carried out using the program Coot (Emsley et al., 2010). Because the Se anomalous data had strong anisotropy and significant twin fraction, a rough model was build based on the anomalous data and the model was subsequently used as the search model to perform molecular replacement for the native data. The molecular replacement and structural refinement were carried out using the program Phenix (Adams et al., 2010). Throughout the refinement, a free R factor was calculated using 5% random chosen reflections. The stereochemistry of the structural models was analyzed using the program Procheck (Laskowski et al., 1993). The structure of NtDRM-M5 was solved using molecular replacement method with the program Phenix and refined with the same protocol as the wild-type protein (Adams et al., 2010). The statistics of the refinement and structure models are shown in Table S1. All the molecular graphics were generated with the program Pymol (DeLano Scientific).

Affinity Purification and Mass Spectrometry

Approximately 10 g flowers from 9xMyc-BLRP-DRM2 or wild-type (WT; negative control) were ground and resuspended in 50 ml of lysis buffer (LB; 50 mM Tris [pH 7.5], 150 mM NaCl, 5 mM MgCl₂, 10% glycerol, 0.1% NP-40, 0.5 mM dithiothreitol [DTT], 1 μg/μl pepstatin, 1 mM phenylmethanesulfonylfluoride [PMSF], and one protease inhibitor cocktail tablet [14696200; Roche]). The resulting crude cell extracts were incubated with 200 μl of monoclonal c-Myc 9E10 agarose beads (AFC-150P; Covance) at 4°C for 2–3 hr. The bead-bound complex was then washed two times with 40 ml of LB and four additional times with 1 ml of LB by mixing at 4°C for 5 min each wash. Bound proteins were released by two times 10 min incubation with 400 μl of 8 M urea at room temperature. The eluted protein complexes were precipitated by trichloroacetic acid and subjected to mass spectrometric analyses as previously described (Du et al., 2012). The interaction between DRM2-AGO4 was performed by using 1.5 g of flowers from Myc-DRM2 transgenic plants and WT plants. The powders were resuspended in 3 ml of low-salt lysis buffer (50 mM Tris [pH 7.5], 50 mM NaCl, 5 mM MgCl₂, 10% glycerol, 0.1% NP-40, 0.5 mM DTT, 1 μg/μl pepstatin, 1 mM PMSF, and one protease inhibitor cocktail tablet). The presence of AGO4 was determined by anti-AGO4 antibody (a gift from Dr. Craig Pikaard, Indiana University) at a dilution of 1:1,000.

Coimmunoprecipitation Analyses

The Nicotiana benthamiana leaves (1.5 g) coexpressing FLAG-tagged and HA-tagged NtDRM MTase were grinded in liquid nitrogen and resuspended in 10 ml of LB buffer. Lysates were cleared by filtration through miracloth followed by centrifugation at 13,200 rpm for 10 min at 4°C. The supernatants were incubated with 50 μl M2 FLAG magnetic beads (50% slurry; Sigma M8823) for 40 min at 4°C with rotation. The beads were then washed five times with 1 ml of LB buffer with incubation of 5 min between each wash. The copurification of HA-DRM was detected by using anti-HA-peroxidase high-affinity 3F10 antibody (13800200; Roche). All western blots were developed using ECL Plus Western Blotting Detection System (RPN2132; GE Healthcare).

DNA Methyltransferase Activity Assays

The methyltransferase assay was modified from previous studies (Du et al., 2012; Wada et al., 2003). Briefly, the activity assay was carried out at room temperature for 1 hr in a total volume of 25 μl containing 2.5 μl of S-adenosyl-l-[methyl-³H] methionine (SAM) (15 Ci/mmol; GE Healthcare), 125 ng substrate DNA, and 100 ng NtDRM protein in assay buffer (20 mM MOPS [pH 7.0], 1 mM DTT, 5 mM EDTA, 200 μg/ml BSA, and 25% glycerol) and stopped by placing tubes into dry ice/ethanol bath and subsequently adding 2 μl of Proteinase K. A total of 10 μl from each reaction was applied onto DE81 paper (Whatman) and washed two times with 200 mM ammonium bicarbonate, two times with water, and two times with ethanol. The paper was dried and placed into liquid scintillation cocktail (Ecolite, MP) and the activity was measured by Beckman scinallation counter, model LS1701 (UK). The DNA oligos JP3010 and JP3011 were annealed and purified as previously described (Du et al., 2012).

Whole-Genome Bisulfite Sequencing

Libraries were prepared as previously described (Stroud et al., 2013) and sequenced on an Illumina HiSeq instrument. Alignment of resulting reads and methods for calculating percent methylation shown in Figure 4A are also as previously described (Stroud et al., 2013). Percent methylation for Figure 3E (complementation of the DRM2-M5 mutant) was calculated similarly, although the reads were aligned using the BSmap program (Xi and Li, 2009). For consistency, the Col WT and DRM2cat data shown in Figure 4A were also remapped with BSmap. The drm2 DMRs were defined as previously described (Greenberg et al., 2013) and the drm2 mutant methylome was previously described (Stroud et al., 2013).

Strand-Specificity Analysis

To define siRNA clusters with a strand bias, we used a previously defined set of total DRM2-dependent siRNA clusters as well as previously published small RNA sequencing data sets (Law et al., 2013) (GSE45368). Small RNA coverage of both the positive and negative strands at these clusters was calculated using unique and nonredundant reads. Strand bias value was calculated as number of aligning reads on the positive strand divided by the number of aligning reads on the negative strand. To avoid artifacts of low coverage, we did not consider clusters that were in the bottom 25th percentile of coverage by small RNA reads. To classify clusters as biased, we chose clusters in the top ten percentiles of bias values (positive-strand bias) and those clusters in the bottom ten percentiles of bias values (negative-strand bias). Neutral clusters (those without strand bias) were defined as clusters with bias values in 40th to 60th percentiles of bias values. Cytosine bias over the resulting groups of small RNA clusters was calculated by simply tallying the number of cytosines on either strand. To calculate methylcytosine bias over these regions, we defined methylcytosines from a wild-type bisulfite library (GSE49090) using a methodology similar to that previously described (Lister et al., 2009) with the exception that a false discovery rate <0.001 was used and the chloroplast genome was used to control for bisulfite conversion efficiency.

To define the hypomethylated cytosines in Figure 6C, we compared a drm2 methylome (GSE39901) to a wild-type methylome (GSE49090) and called individual hypomethylated cytosines of as those significantly hypomethylated (p < 0.001, Fisher's exact test). The other methyltransferase methylomes were published previously (GSE39901). To avoid oversampling, small RNA profiles from clusters of hypomethylated cytosines groups of DMCs within 24 nt of each other were sampled as to only have one DMC. Small RNA reads from three wild-type libraries (Law et al., 2013; Stroud et al., 2014) (GSE45368, GSE49090, and GSE52041) were plotted about these identified hypomethylated cytosines.

ACCESSION NUMBERS

Coordinates and structure factors for NtDRM MTase domain and NtDRM-M5, both in the presence of sinefungin, have been deposited in the RCSB Protein Data Bank with the accession codes 4ONJ and 4ONQ, respectively. Sequencing data were deposited to the NCBI Gene Expression Omnibus with the accession number GSE54944.

SUPPLEMENTAL INFORMATION

Supplemental Information includes five figures and two tables and can be found with this article online at http://dx.doi.org/10.1016/j.cell.2014.03.056.

REFERENCES

Adams, P.D., Afonine, P.V., Bunkóczi, G., Chen, V.B., Davis, I.W., Echols, N., Headd, J.J., Hung, L.W., Kapral, G.J., Grosse-Kunstleve, R.W., et al. (2010). PHENIX: a comprehensive Python-based system for macromolecular structure solution. Acta Crystallogr. D Biol. Crystallogr. 66, 213–221.

Cao, X., and Jacobsen, S.E. (2002). Role of the arabidopsis DRM methyltransferases in de novo DNA methylation and gene silencing. Curr. Biol. 12, 1138–1144.

Cao, X., Springer, N.M., Muszynski, M.G., Phillips, R.L., Kaeppler, S., and Jacobsen, S.E. (2000). Conserved plant genes with similarity to mammalian de novo DNA methyltransferases. Proc. Natl. Acad. Sci. USA 97, 4979–4984.

Cheng, X., Kumar, S., Posfai, J., Pflugrath, J.W., and Roberts, R.J. (1993). Crystal structure of the HhaI DNA methyltransferase complexed with S-adenosyl-L-methionine. Cell 74, 299–307.

Cokus, S.J., Feng, S., Zhang, X., Chen, Z., Merriman, B., Haudenschild, C.D., Pradhan, S., Nelson, S.F., Pellegrini, M., and Jacobsen, S.E. (2008). Shotgun bisulphite sequencing of the Arabidopsis genome reveals DNA methylation patterning. Nature 452, 215–219.

Du, J., Zhong, X., Bernatavichute, Y.V., Stroud, H., Feng, S., Caro, E., Vashisht, A.A., Terragni, J., Chin, H.G., Tu, A., et al. (2012). Dual binding of chromomethylase domains to H3K9me2-containing nucleosomes directs DNA methylation in plants. Cell 151, 167–180.

Earley, K.W., Haag, J.R., Pontes, O., Opper, K., Juehne, T., Song, K., and Pikaard, C.S. (2006). Gateway-compatible vectors for plant functional genomics and proteomics. Plant J. 45, 616–629.

El-Shami, M., Pontier, D., Lahmy, S., Braun, L., Picart, C., Vega, D., Hakimi, M.A., Jacobsen, S.E., Cooke, R., and Lagrange, T. (2007). Reiterated WG/GW motifs form functionally and evolutionarily conserved ARGONAUTE-binding platforms in RNAi-related components. Genes Dev. 21, 2539–2544.

Emsley, P., Lohkamp, B., Scott, W.G., and Cowtan, K. (2010). Features and development of Coot. Acta Crystallogr. D Biol. Crystallogr. 66, 486–501.

Finnegan, E.J., and Dennis, E.S. (1993). Isolation and identification by sequence homology of a putative cytosine methyltransferase from Arabidopsis thaliana. Nucleic Acids Res. 21, 2383–2388.

Finnegan, E.J., and Kovac, K.A. (2000). Plant DNA methyltransferases. Plant Mol. Biol. 43, 189–201.

Greenberg, M.V., Deleris, A., Hale, C.J., Liu, A., Feng, S., and Jacobsen, S.E. (2013). Interplay between active chromatin marks and RNA-directed DNA methylation in Arabidopsis thaliana. PLoS Genet. 9, e1003946.

Henderson, I.R., Deleris, A., Wong, W., Zhong, X., Chin, H.G., Horwitz, G.A., Kelly, K.A., Pradhan, S., and Jacobsen, S.E. (2010). The de novo cytosine methyltransferase DRM2 requires intact UBA domains and a catalytically mutated paralog DRM3 during RNA-directed DNA methylation in Arabidopsis thaliana. PLoS Genet. 6, e1001182.

Jia, D., Jurkowska, R.Z., Zhang, X., Jeltsch, A., and Cheng, X. (2007). Structure of Dnmt3a bound to Dnmt3L suggests a model for de novo DNA methylation. Nature 449, 248–251.

Johnson, L.M., Du, J., Hale, C.J., Bischof, S., Feng, S., Chodavarapu, R.K., Zhong, X., Marson, G., Pellegrini, M., Segal, D.J., et al. (2014). SRA- and SET-domain-containing proteins link RNA polymerase V occupancy to DNA methylation. Nature 507, 124–128.

Laskowski, R.A., Macarthur, M.W., Moss, D.S., and Thornton, J.M. (1993). PROCHECK: a program to check the stereochemical quality of protein structures. J. Appl. Cryst. 26, 283–291.

Law, J.A., and Jacobsen, S.E. (2010). Establishing, maintaining and modifying DNA methylation patterns in plants and animals. Nat. Rev. Genet. 11, 204–220.

Law, J.A., Du, J., Hale, C.J., Feng, S., Krajewski, K., Palanca, A.M., Strahl, B.D., Patel, D.J., and Jacobsen, S.E. (2013). Polymerase IV occupancy at RNA-directed DNA methylation sites requires SHH1. Nature 498, 385–389.

Lee, T.F., Gurazada, S.G., Zhai, J., Li, S., Simon, S.A., Matzke, M.A., Chen, X., and Meyers, B.C. (2012). RNA polymerase V-dependent small RNAs in Arabidopsis originate from small, intergenic loci including most SINE repeats. Epigenetics 7, 781–795.

Li, C.F., Pontes, O., El-Shami, M., Henderson, I.R., Bernatavichute, Y.V., Chan, S.W., Lagrange, T., Pikaard, C.S., and Jacobsen, S.E. (2006). An ARGONAUTE4-containing nuclear processing center colocalized with Cajal bodies in Arabidopsis thaliana. Cell 126, 93–106.

Lindroth, A.M., Cao, X., Jackson, J.P., Zilberman, D., McCallum, C.M., Henikoff, S., and Jacobsen, S.E. (2001). Requirement of CHROMOMETHYLASE3 for maintenance of CpXpG methylation. Science 292, 2077–2080.

Lister, R., O'Malley, R.C., Tonti-Filippini, J., Gregory, B.D., Berry, C.C., Millar, A.H., and Ecker, J.R. (2008). Highly integrated single-base resolution maps of the epigenome in Arabidopsis. Cell 133, 523–536.

Lister, R., Pelizzola, M., Dowen, R.H., Hawkins, R.D., Hon, G., Tonti-Filippini, J., Nery, J.R., Lee, L., Ye, Z., Ngo, Q.M., et al. (2009). Human DNA methylomes at base resolution show widespread epigenomic differences. Nature 462, 315–322.

Luo, S., and Preuss, D. (2003). Strand-biased DNA methylation associated with centromeric regions in Arabidopsis. Proc. Natl. Acad. Sci. USA 100, 11133–11138.

Otwinowski, Z., and Minor, W. (1997). Processing of X-ray Diffraction Data Collected in Oscillation Mode. Methods Enzymol. 276, 307–326.

Qi, Y., He, X., Wang, X.J., Kohany, O., Jurka, J., and Hannon, G.J. (2006). Distinct catalytic and non-catalytic roles of ARGONAUTE4 in RNA-directed DNA methylation. Nature 443, 1008–1012.

Schubert, H.L., Blumenthal, R.M., and Cheng, X. (2003). Many paths to methyltransfer: a chronicle of convergence. Trends Biochem. Sci. 28, 329–335.

Song, J., Rechkoblit, O., Bestor, T.H., and Patel, D.J. (2011). Structure of DNMT1-DNA complex reveals a role for autoinhibition in maintenance DNA methylation. Science 331, 1036–1040.

Song, J., Teplova, M., Ishibe-Murakami, S., and Patel, D.J. (2012). Structure-based mechanistic insights into DNMT1-mediated maintenance DNA methylation. Science *335*, 709–712.

Stroud, H., Greenberg, M.V., Feng, S., Bernatavichute, Y.V., and Jacobsen, S.E. (2013). Comprehensive analysis of silencing mutants reveals complex regulation of the Arabidopsis methylome. Cell *152*, 352–364.

Stroud, H., Do, T., Du, J., Zhong, X., Feng, S., Johnson, L., Patel, D.J., and Jacobsen, S.E. (2014). Non-CG methylation patterns shape the epigenetic landscape in Arabidopsis. Nat. Struct. Mol. Biol. *21*, 64–72.

Wada, Y., Ohya, H., Yamaguchi, Y., Koizumi, N., and Sano, H. (2003). Preferential de novo methylation of cytosine residues in non-CpG sequences by a domains rearranged DNA methyltransferase from tobacco plants. J. Biol. Chem. *278*, 42386–42393.

Wierzbicki, A.T., Ream, T.S., Haag, J.R., and Pikaard, C.S. (2009). RNA polymerase V transcription guides ARGONAUTE4 to chromatin. Nat. Genet. *41*, 630–634.

Xi, Y., and Li, W. (2009). BSMAP: whole genome bisulfite sequence MAPping program. BMC Bioinformatics *10*, 232.

Zemach, A., Kim, M.Y., Hsieh, P.H., Coleman-Derr, D., Eshed-Williams, L., Thao, K., Harmer, S.L., and Zilberman, D. (2013). The Arabidopsis nucleosome remodeler DDM1 allows DNA methyltransferases to access H1-containing heterochromatin. Cell *153*, 193–205.

Zhang, H., Ma, Z.Y., Zeng, L., Tanaka, K., Zhang, C.J., Ma, J., Bai, G., Wang, P., Zhang, S.W., Liu, Z.W., et al. (2013). DTF1 is a core component of RNA-directed DNA methylation and may assist in the recruitment of Pol IV. Proc. Natl. Acad. Sci. USA *110*, 8290–8295.

Zhong, X., Hale, C.J., Law, J.A., Johnson, L.M., Feng, S., Tu, A., and Jacobsen, S.E. (2012). DDR complex facilitates global association of RNA polymerase V to promoters and evolutionarily young transposons. Nat. Struct. Mol. Biol. *19*, 870–875.